Inorg. Chem. **2003**, *42*, 8572–8578

Short-Range and Long-Range Magnetic Ordering in $SrCuP_2O_7$ and $PbCuP_2O_7$

Alexei A. Belik,*,† Masaki Azuma,†,‡ and Mikio Takano†

Institute for Chemical Research, Kyoto University, Uji, Kyoto-fu 611-0011, Japan, and PRESTO, Japan Science and Technology Corporation (JST), Kawaguchi, Saitama 332-0012, Japan

Received July 15, 2003

Magnetic properties of $SrCuP_2O_7$ and $PbCu_{1-x}Zn_xP_2O_7$ ($x = 0$, 0.1, and 0.5) were studied by magnetic susceptibility, $\chi(T)$, and specific heat, $C_p(T)$. Both data showed that magnetism of $SrCuP_2O_7$ and $PbCuP_2O_7$ can be described by the one-dimensional (1D) uniform chain model despite the structural features suggesting the presence of zigzag chains with next-nearest-neighbor interactions. The $\chi(T)$ data were fitted by the Bonner–Fisher curve (plus temperature independent and Curie–Weiss terms) with $g = 2.20$ and $J/k_B = 9.38$ K for $SrCuP_2O_7$ and $g = 2.17$ and $J/k_B = 8.41$ K for $PbCuP_2O_7$ (Hamiltonian $H = J \Sigma S_i S_{i+1}$). Magnetic specific heat, $C_m(T)$, exhibited one broad maximum due to short-range ordering and one sharp peak at $T_N = 1.64$ K for $SrCuP_2O_7$ and $T_N = 1.15$ K for $PbCuP_2O_7$ due to long-range antiferromagnetic ordering. The characteristic values of the broad maxima on the $C_m(T)$ curves (C_{max} and T^C_{max}) were in good agreement with the theoretical calculations for the uniform 1D $S = 1/2$ Heisenberg chain. Magnetic properties of $PbCu_{0.9}Zn_{0.1}P_2O_7$ still obeyed the 1D uniform chain model but those of $PbCu_{0.5}Zn_{0.5}P_2O_7$ did not. In air, $SrCuP_2O_7$ was stable at least up to 1373 K while $PbCuP_2O_7$ melted incongruently above 1180 K.

Introduction

Low-dimensional quantum magnets have attracted considerable attention because of interesting physical properties. For example, the spin-Peierls transition observed in some organic compounds and in $CuGeO_3$[1] is one of the quantum phenomena in a one-dimensional (1D) $S = 1/2$ antiferromagnetic (AF) Heisenberg chain. Below the critical temperature, a finite energy gap opens in the magnetic excitation spectrum accompanying with a lattice distortion (lattice dimerization), and the spin system is in a spin-singlet state. Spin-singlet ground states with finite gaps have also been found in other 1D AF systems: $S = 1/2$ alternating bond chains,[2,3] e.g., $(VO)_2P_2O_7$,[4] $S = 1/2$ two-leg ladders,[5] e.g., $SrCu_2O_3$[6,7] and $Sr_{14}Cu_{24}O_{41}$,[8] and $S = 1$ chains,[9] e.g., Y_2BaNiO_5[10] and $PbNi_2V_2O_8$[11] (Haldane systems).

Quantum fluctuations in the $S = 1/2$ uniform Heisenberg chain are so strong that the ground state is disordered while the excitation spectrum is gapless. Ideal 1D gapless systems do not undergo three-dimensional (3D) magnetic ordering. However, in a real compound, finite interchain coupling leads to the 3D ordered ground state with spontaneous sublattice magnetization.

Quantum phenomena in a 1D zigzag chain with the next-nearest-neighbor (NNN) interaction have recently been studied from both theoretical and experimental viewpoints.[12−17]

* To whom correspondence should be addressed. E-mail: belik@msk.kuicr.kyoto-u.ac.jp. Phone: +81-774-38-3122. Fax: +81-774-38-3125.
† Institute for Chemical Research.
‡ PRESTO.

(1) Hase, M.; Terasaki, I.; Uchinokura, K. *Phys. Rev. Lett.* **1993**, *70*, 3651−3654.
(2) Bonner, J. C.; Fisher, M. E. *Phys. Rev. A* **1964**, *135*, 640−658.
(3) (a) Bonner, J. C.; Blöte, H. W. J.; Bray, J. W.; Jacobs, I. S. *J. Appl. Phys.* **1979**, *50*, 1810−1812. (b) Bonner, J. C.; Blöte, H. W. J. *Phys. Rev. B* **1982**, *25*, 6959−6980.
(4) (a) Kikuchi, J.; Motoya, K.; Yamauchi, T.; Ueda, Y. *Phys. Rev. B* **1999**, *60*, 6731−6739. (b) Azuma, M.; Saito, T.; Fujishiro, Y.; Hiroi, Z.; Takano, M.; Izumi, F.; Kamiyama, T.; Ikeda, T.; Narumi, Y.; Kindo, K. *Phys. Rev. B* **1999**, *60*, 10145−10149.
(5) Dagotto, E.; Rice, T. M. *Science* **1996**, *271*, 618−623.
(6) (a) Hiroi, Z.; Azuma, M.; Takano, M.; Bando, Y. *J. Solid State Chem.* **1991**, *95*, 230−238. (b) Azuma, M.; Hiroi, Z.; Takano, M.; Ishida, K.; Kitaoka, Y. *Phys. Rev. Lett.* **1994**, *73*, 3463−3466.
(7) Azuma, M.; Takano, M.; Eccleston, R. S. *J. Phys. Soc. Jpn.* **1998**, *67*, 740−743.
(8) Eccleston, R. S.; Uehara, M.; Akimitsu, J.; Eisaki, H.; Motoyama, N.; Uchida, S. *Phys. Rev. Lett.* **1998**, *81*, 1702−1705.
(9) Haldane, F. D. M. *Phys. Rev. Lett.* **1983**, *50*, 1153−1156.
(10) Darriet, J.; Regnault, L. P. *Solid State Commun.* **1993**, *86*, 409−412.
(11) Uchiyama, Y.; Sasago, Y.; Tsukada, I.; Uchinokura, K.; Zheludev, A.; Hayashi, T.; Miura, N.; Böni, P. *Phys. Rev. Lett.* **1999**, *83*, 632−635.
(12) Maeshima, N.; Okunishi, K. *Phys. Rev. B* **2000**, *62*, 934−939.
(13) Hosokoshi, Y.; Katoh, K.; Inoue, K.; Goto, T. *J. Phys. Soc. Jpn.* **1999**, *68*, 2910−2913.
(14) Hagiwara, M.; Narumi, Y.; Kindo, K.; Maeshima, N.; Okunishi, K.; Sakai, T.; Takahashi, M. *Physica B* **2001**, *294*−*295*, 83−86.

10.1021/ic034825w CCC: $25.00
Published on Web 11/15/2003

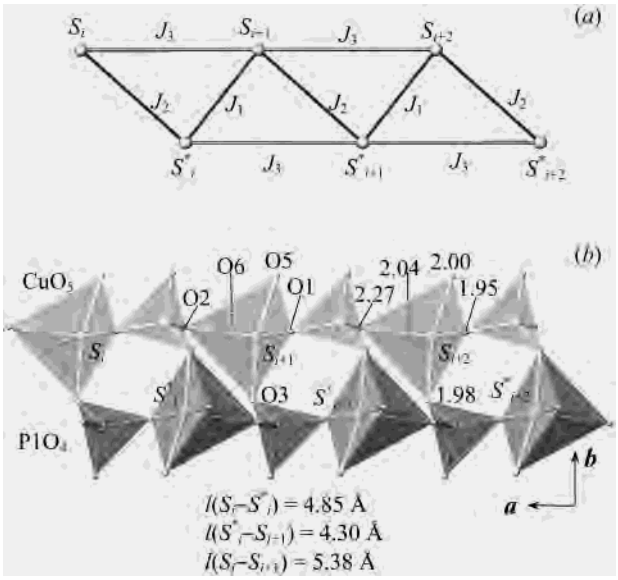

Figure 1. (a) Spin interaction scheme for the bond-alternating zigzag chain with the next-nearest-neighbor interaction. (b) Projection of the structure of $PbCuP_2O_7$ along the *c* direction emphasizing the Cu−Cu chains. Pb atoms and $P2O_4$ tetrahedra were removed for the clarity. Cu−O distances are given in Å.

Spin interactions in such systems shown in Figure 1a are described by three exchange constants (J_1, J_2, and J_3). This model is also called the double-spin chain model.[15,16] Depending on the ratio between J_1, J_2, and J_3, this spin system can have a gapped ground state or can be gapless. In the case of $J_1 = J_2$, it gives the so-called railroad-trestle model.[12−14] For $J_2 = 0$, the ordinary two-leg ladder system is obtained.

$SrCuP_2O_7$[18] and $PbCuP_2O_7$[19] are the candidate model compounds for the $S = {}^1/_2$ zigzag chain with NNN interactions. They are isotypic with α-$Ca_2P_2O_7$ crystallizing in space group $P2_1/n$ with $a \approx 5.4$ Å, $b \approx 8.1$ Å, $c \approx 12.5$ Å, and $\beta \approx 90.5°$.[19] Cu^{2+} ions with $S = {}^1/_2$ have square pyramidal coordinations. There is no direct Cu−O−Cu interaction, but Cu atoms are connected with each other through O−P−O bonds of PO_4 groups. The copper framework in the structures of $SrCuP_2O_7$ and $PbCuP_2O_7$ can be described in three ways. The first description is 1D bond-alternating zigzag chains along the *a* axis (Figure 1b). Cu atoms in the zigzag chain are connected with each other by two O−P−O bonds with Cu−Cu distances of 4.30 and 4.85 Å (for $PbCuP_2O_7$). Cu atoms in the zigzag chain have also the NNN interaction transferred through one O−P−O bond with the Cu−Cu distance of 5.38 Å (for $PbCuP_2O_7$). This model fails into a dimer system when J_2 is dominant (the second model). The third description is 1D uniform zigzag chains along the *b* axis (Figure 2). In this case, Cu atoms with the nearest-neighbor (NN) interaction (J_4) are connected by one O−P−O bond with the Cu−Cu distance of 5.38 Å (for $PbCuP_2O_7$), and the NNN interactions (J_5) are mediated by the two PO_4 tetrahedra (or one P_2O_7 group).

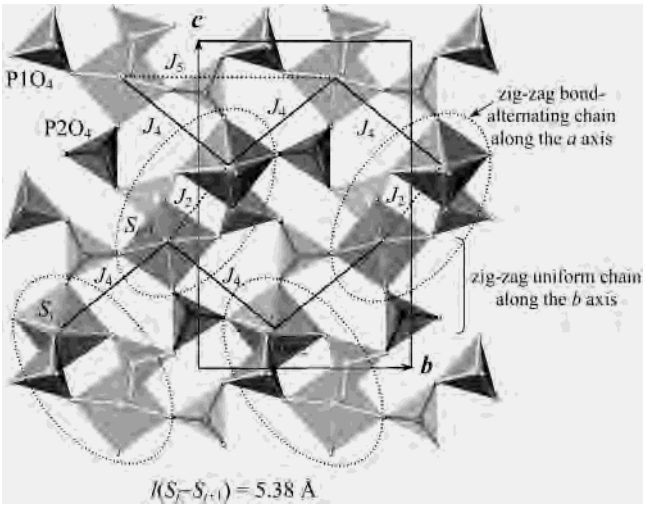

Figure 2. Projection of the structure of $PbCuP_2O_7$ along the *a* direction. Pb atoms are not shown.

$CaCuP_2O_7$,[20] $BaCuAs_2O_7$,[21] and other compounds with the general formula of ABC_2O_7 (e.g., $SrZnP_2O_7$ and $PbZnP_2O_7$) are also isotypic with α-$Ca_2P_2O_7$.[22] Magnetic susceptibilities were measured for $CaCuP_2O_7$ and $SrCuP_2O_7$ in the temperature range 4.2−300 K, but only the Curie−Weiss behavior was reported.[23] In this work, we have studied properties of $SrCuP_2O_7$, $PbCuP_2O_7$, and solid solutions $PbCu_{1-x}Zn_xP_2O_7$ ($0 \le x \le 1$) by magnetic susceptibility and specific heat measurements. The experimental data agreed well with the assumption of the presence of the 1D uniform zigzag chains with almost negligible NNN interactions. We have observed short-range and long-range magnetic ordering in $SrCuP_2O_7$ and $PbCuP_2O_7$ and also investigated the thermal stability of these two compounds in air.

Experimental Section

Synthesis. $SrCuP_2O_7$, $PbCuP_2O_7$, $SrZnP_2O_7$, and $PbZnP_2O_7$ were prepared from stoichiometric mixtures of $SrCO_3$ (99.99%), PbO (99.9%), ZnO (99.9%), CuO (99.99%), and $NH_4H_2PO_4$ (99.8%) by the solid state method in alumina crucibles. The mixtures were heated very slowly from room temperature to 770 K, reground, and then allowed to react at 1173 K for $SrCuP_2O_7$ and $SrZnP_2O_7$ and at 973 K for $PbCuP_2O_7$ and $PbZnP_2O_7$ for 100 h with four intermediate grindings. Solid solutions $PbCu_{1-x}Zn_xP_2O_7$ with $x =$ 0.1 and 0.5 were prepared from stoichiometric mixtures of $PbCuP_2O_7$ and $PbZnP_2O_7$ at 973 K for 80 h with two intermediate grindings. X-ray powder diffraction (XRD) data collected with a RIGAKU RINT 2500 diffractometer (2θ range of 8−60°, a step width of 0.02°, and a counting time of 1 s/step) showed that all the samples were monophasic.

(15) Nakamura, T.; Okamoto, K. *Phys. Rev. B* **1998**, *58*, 2411−2414.
(16) Nakamura, T. *Phys. Rev. B* **1998**, *57*, R3197−R3200.
(17) Haga, N.; Suga, S.-I. *Phys. Rev. B* **2001**, *65*, 014414-1−014414-7.
(18) Moqine, A.; Boukhari, A.; Elammari, L.; Durand, J. *J. Solid State Chem.* **1993**, *107*, 368−372.
(19) Elmarzouki, A.; Boukhari, A.; Holt, E. M.; Berrada, A. *J. Alloys Compd.* **1995**, *227*, 125−130.
(20) Riou, D.; Goreaud, M. *Acta Crystallogr., Sect. C* **1990**, *46*, 1191−1193.
(21) (a) Wardojo, T. A.; Hwu, S.-J. *J. Solid State Chem.* **1995**, *118*, 280−284. (b) Chen, T.-C.; Wang, S.-L. *J. Solid State Chem.* **1996**, *121*, 350−355.
(22) Maass, K.; Glaum, R. *Acta Crystallogr., Sect. C* **2000**, *56*, 404−406.
(23) Boukhari, A.; Moqine, A.; Flandrois, S. *J. Solid State Chem.* **1990**, *87*, 251−256.

Table 1. Fitted Parameters for $\chi^{-1}(T)$ and $\chi(T)$ of $SrCuP_2O_7$, $PbCuP_2O_7$, and $PbCu_{1-x}Zn_xP_2O_7$

			$PbCu_{1-x}Zn_xP_2O_7$		
eq	quantity	$SrCuP_2O_7$	$x = 0.0$	$x = 0.1$	$x = 0.5$
eq 1	temp range (K)	15−400	15−400	15−400	15−400
	χ_0 (cm^3/Cu mol)	$-2.76(2) \times 10^{-4}$	$-5.60(10) \times 10^{-5}$	$-4.90(2) \times 10^{-4}$	$-5.78(2) \times 10^{-4}$
	C (cm^3K/Cu mol)	0.4371(8)	0.4229(4)	0.4395(9)	0.4341(10)
	θ (K)	−4.04(14)	−3.53(8)	−3.35(19)	−1.29(22)
eqs 2 and 3	temp range (K)	2−400	2−400	2−400	
	χ_0 (cm^3/Cu mol)	$-3.34(3) \times 10^{-4}$	$-1.34(4) \times 10^{-4}$	$-5.87(5) \times 10^{-4}$	
	C_{imp} (cm^3 K/Cu mol)	$2.53(9) \times 10^{-3}$	$2.64(8) \times 10^{-3}$	$1.96(5) \times 10^{-2}$	
	θ_{imp} (K)	1.11(3)	1.43(2)	0.20(4)	
	g	2.1999(4)	2.1689(5)	2.1746(11)	
	J/k_B[a] (K)	9.378(6)	8.410(8)	8.134(14)	
	σ_{rms}[b] (%)	0.544	1.034	1.979	
	R[c]	2.31×10^{-6}	6.02×10^{-6}	3.17×10^{-6}	

[a] Hamiltonian $H = J \Sigma S_i S_{i+1}$.

[b] $\sigma^2_{rms} = \frac{1}{N_p}\sum_{i=1}^{N_p}\left[\frac{(\chi(T_i) - \chi_{fit}(T_i))}{\chi(T_i)}\right]^2$ where N_p is the number of data points.

[c] $R = \frac{\sum_{i=1}^{N_p}(\chi(T_i) - \chi_{fit}(T_i))^2}{\sum_{i=1}^{N_p}(\chi(T_i))^2}$.

Magnetic and Specific Heat Measurements. Magnetic susceptibilities, χ, of $SrCuP_2O_7$, $PbCuP_2O_7$, and $PbCu_{1-x}Zn_xP_2O_7$ were measured on a SQUID magnetometer (Quantum Design, MPMS XL) between 2 and 400 K in an applied field of 100 Oe under both zero-field-cooled (ZFC) and field-cooled (FC) conditions. Specific heat, C_p, was recorded between 0.45 and 21 K (on cooling) by a pulse relaxation method using a commercial calorimeter (Quantum Design PPMS).

Thermal Analysis. Thermal stability of $SrCuP_2O_7$ and $PbCuP_2O_7$ was examined under air with a MacScience TG-DTA 2000 instrument. The samples were placed in Pt crucibles, heated, and then cooled with a rate of 10 K/min. $SrCuP_2O_7$ was heated to 1373 K, but differential thermal analysis (DTA) showed no thermal effects. XRD data confirmed that the sample remained monophasic. $PbCuP_2O_7$ was heated to 1213 K. DTA data showed two peaks centered at 1186 and 1190 K on heating and three peaks centered at 1013, 1029, and 1163 K on cooling. Such inconsistence of heating and cooling behavior suggested that $PbCuP_2O_7$ melted incongruently above 1180 K.

Results and Discussion

Figure 3 presents plots of χ and χ^{-1} (ZFC curves) against temperature, T, for $SrCuP_2O_7$ and $PbCuP_2O_7$. No noticeable difference was found between the curves measured under the ZFC and FC conditions. The $\chi(T)$ data exhibited a broad maximum at $T_M = 6.0$ K for $SrCuP_2O_7$ and $T_M = 5.2$ K for $PbCuP_2O_7$ characteristic of quasi-1D systems. Above 15 K, the $\chi^{-1}(T)$ data obeyed the Curie−Weiss rule including the temperature-independent term (χ_0)

$$\chi(T) = \chi_0 + \frac{C}{T - \theta} \quad (1)$$

where C is the Curie constant and θ is the Weiss constant. The fitted parameters to eq 1 are given in Table 1.

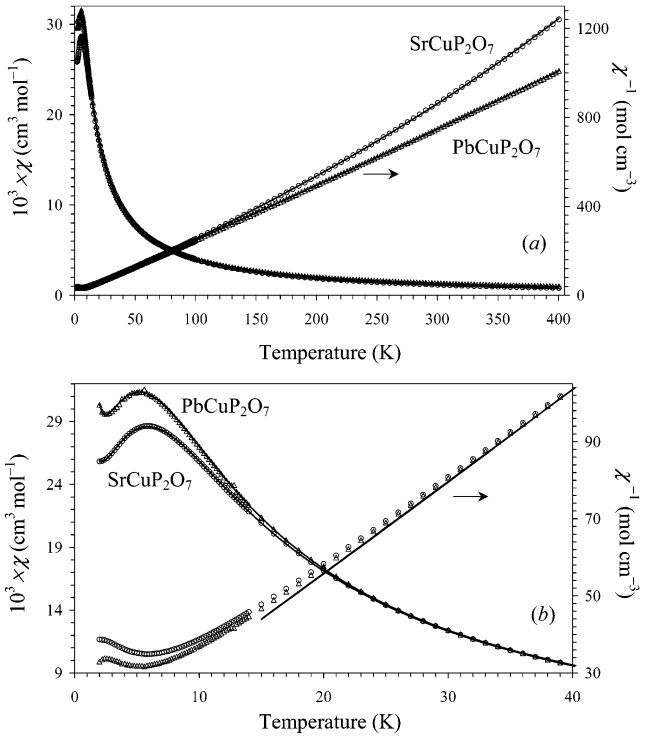

Figure 3. Magnetic susceptibilities, χ and χ^{-1} (ZFC curves), against temperature, T, for $SrCuP_2O_7$ and $PbCuP_2O_7$. Solid lines represent fits by eq 1 for the χ^{-1} data and by eqs 2 and 3 for the χ data. (b) Enlarged fragment shown in part a.

The $\chi(T)$ data did not exhibit vanishing behavior below T_M characteristic of spin gap compounds but tended to approach finite values typical for gapless quasi-1D systems. Indeed, the $\chi(T)$ data were fitted very well in the entire temperature range by the equations for the uniform 1D

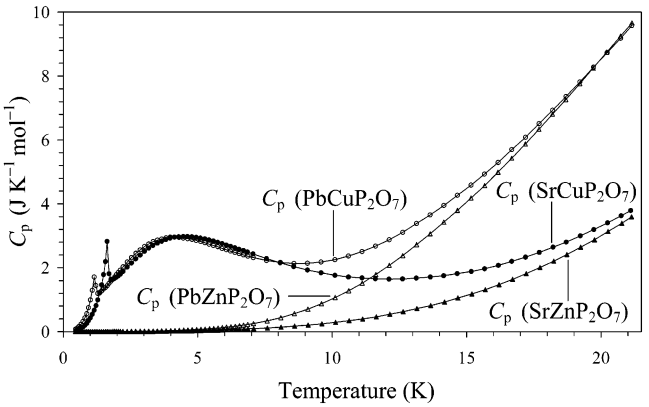

Figure 4. Total specific heat, C_p, plotted against temperature, T, for $SrCuP_2O_7$, $SrZnP_2O_7$, $PbCuP_2O_7$, and $PbZnP_2O_7$. Solid lines are drawn for the eye.

Heisenberg AF chain

$$\chi(T) = \chi_0 + C_{imp}/(T - \theta_{imp}) + \chi_{chain}(T) \quad (2)$$

$$\chi_{chain}(T) = \frac{Ng^2\mu_B{}^2}{k_BT} \frac{0.25 + 0.14995x + 0.30094x^2}{1 + 1.9862x + 0.68854x^2 + 6.0626x^3} \quad (3)$$

where $\chi_{chain}(T)$ is the Bonner−Fisher curve[2] parametrized by Estes et al.,[24] $x \equiv J/(2k_BT)$, N is Avogadro's number, g is the spectroscopic splitting factor (g-factor), μ_B is the Bohr magneton, k_B is Boltzmann's constant, C_{imp} is an impurity Curie constant, and θ_{imp} is an impurity Weiss constant. The fitted parameters and measures of the quantity of fits (σ_{rms} and R) are also given in Table 1.

Specific heat data were taken at zero field to assess the effect of possible NNN interactions and interchain interactions in $SrCuP_2O_7$ and $PbCuP_2O_7$. The total specific heat values plotted against temperature, $C_p(T)$, for $SrCuP_2O_7$, $SrZnP_2O_7$, $PbCuP_2O_7$, and $PbZnP_2O_7$ are shown in Figure 4. Since these are insulators, there is no electronic specific heat. If we assume that lattice contributions to the specific heat are the same for $SrCuP_2O_7$ and $SrZnP_2O_7$ and for $PbCuP_2O_7$ and $PbZnP_2O_7$, the magnetic specific heat, $C_m(T)$, for $SrCuP_2O_7$ can be obtained by subtracting the total specific heat of $SrZnP_2O_7$ from that of $SrCuP_2O_7$, and $C_m(T)$ for $PbCuP_2O_7$ can be obtained by subtracting $C_p(T)$ of $PbZnP_2O_7$ from that of $PbCuP_2O_7$.

The $C_m(T)$ curves (Figure 5) exhibited broad maxima with values of C_{max} at temperatures T^C_{max} (C_{max} = 2.951 J K^{-1} mol^{-1} and T^C_{max} = 4.46 K for $SrCuP_2O_7$ and C_{max} = 2.922 J K^{-1} mol^{-1} and T^C_{max} = 3.98 K for $PbCuP_2O_7$) due to short-range magnetic ordering and sharp peaks at T_N (T_N = 1.64 K for $SrCuP_2O_7$ and T_N = 1.15 K for $PbCuP_2O_7$) due to long-range magnetic ordering. The calculated magnetic specific heat, $(C_m)_{calc}$, for the $S = 1/2$ AF uniform Heisenberg chain with the J/k_B parameters determined from the $\chi(T)$ data are also plotted in Figure 5. For the calculations of $(C_m)_{calc}$, we used eq 54 of ref 25.

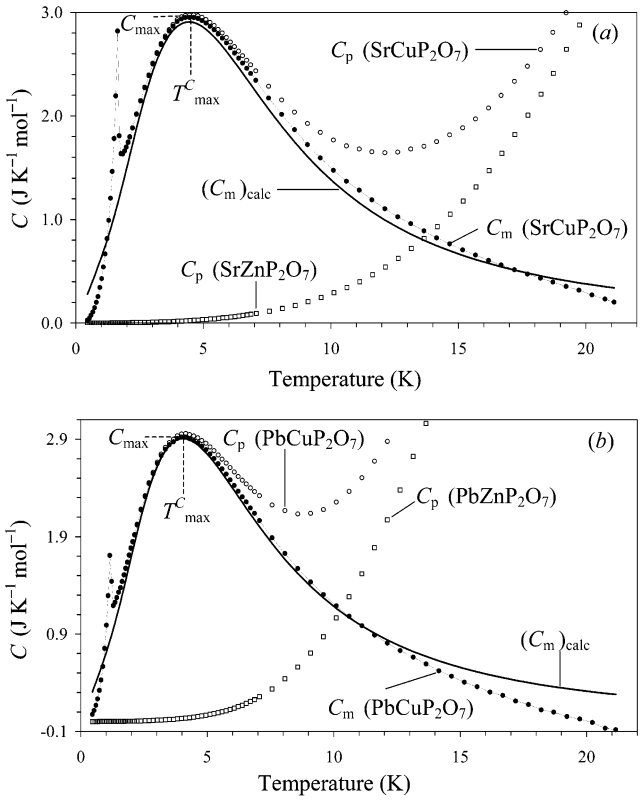

Figure 5. Magnetic specific heat, C_m, plotted against T for (a) $SrCuP_2O_7$ and (b) $PbCuP_2O_7$. Thin solid lines between experimental points are drawn for the eye. Thick solid lines are the calculated magnetic specific heat, $(C_m)_{calc}$, for the $S = 1/2$ uniform chain model with the J/k_B parameters determined from the $\chi(T)$ data. The characteristic values of the broad maxima (C_{max} and T^C_{max}) are shown. Total specific heat is also drawn for comparison.

T^C_{max}'s were in excellent agreement with the theoretical values, $(T^C_{max})_{calc} \approx 0.4803(J/k_B)$,[25] with the J/k_B parameters determined from the $\chi(T)$ data ($(T^C_{max})_{calc}$ = 4.51 K for $SrCuP_2O_7$ and $(T^C_{max})_{calc}$ = 4.04 K for $PbCuP_2O_7$). C_{max}'s were also consistent with the theoretical prediction, $(C_{max})_{calc} \approx 0.3497Nk_B$ = 2.908 J K^{-1} mol^{-1}.[25]

Because of the presence of the interchain interactions, the systems underwent AF long-range orderings. Figure 6 shows the magnetic specific heat divided by temperature, $C_m(T)/T$, and the magnetic entropy, $S_m(T) = \int(C_m/T)\,dT$, curves. $S_m(T)$ values approached $R \ln 2 \approx 5.76$ J K^{-1} mol^{-1}, expected for the $S = 1/2$ systems, where R is the molar gas constant, but only 12.0% (for $SrCuP_2O_7$) and 8.1% (for $PbCuP_2O_7$) of the saturation value was gained at T_N reflecting the 1D nature of the systems.

Figure 7 depicts the $\chi(T)$ and $C_m(T)/T$ data for $PbCu_{1-x}Zn_xP_2O_7$ (x = 0, 0.1, and 0.5). The $C_m(T)/T$ data evidenced that long-range ordering with T_N = 1.15 K was suppressed with increasing x. For example, for x = 0.1, the peak at 1.15 K was still observed whereas for x = 0.5, no long-range ordering was detected. Note that the $C_m(T)/T$ values started to increase below 0.7 K for $PbCu_{0.5}Zn_{0.5}P_2O_7$ suggesting the presence of T_N at a lower temperature. Short-range correlations persisted for x = 0.1 and 0.5 as clearly seen on the

(24) Estes, W. E.; Gavel, D. P.; Hatfield, W. E.; Hodgson, D. J. *Inorg. Chem.* **1978**, *17*, 1415−1421.

(25) Johnston, D. C.; Kremer, R. K.; Troyer, M.; Wang, X.; Klümper, A.; Bud'ko, S. L.; Panchula, A. F.; Canfield, P. C. *Phys. Rev. B* **2000**, *61*, 9558−9606.

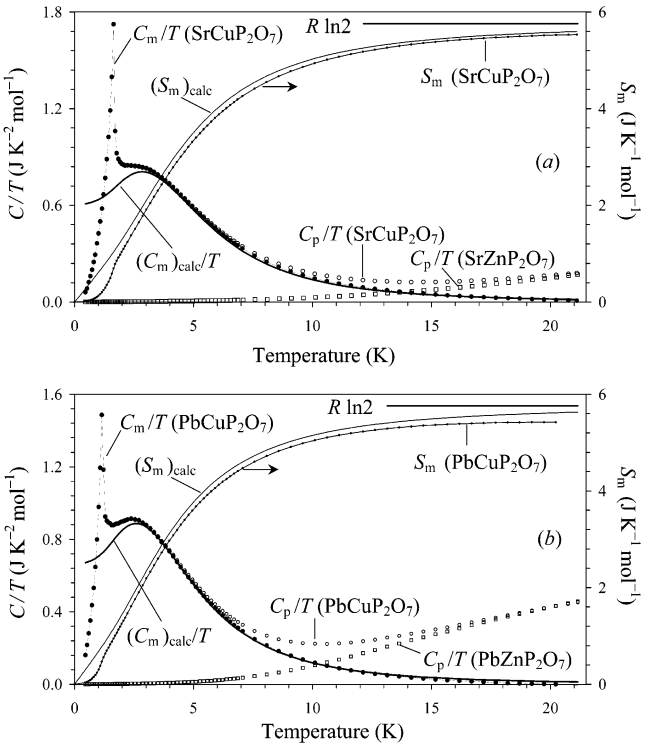

Figure 6. Magnetic specific heat divided by temperature, C_m/T, and magnetic entropy, S_m, plotted against T for (a) $SrCuP_2O_7$ and (b) $PbCuP_2O_7$. Thin solid lines between experimental points are drawn for the eye. Thick solid lines are the calculated magnetic specific heat divided by temperature, $(C_m)_{calc}/T$. $(S_m)_{calc} = \int((C_m)_{calc}/T)\,dT$. Total specific heat divided by temperature is also drawn for comparison.

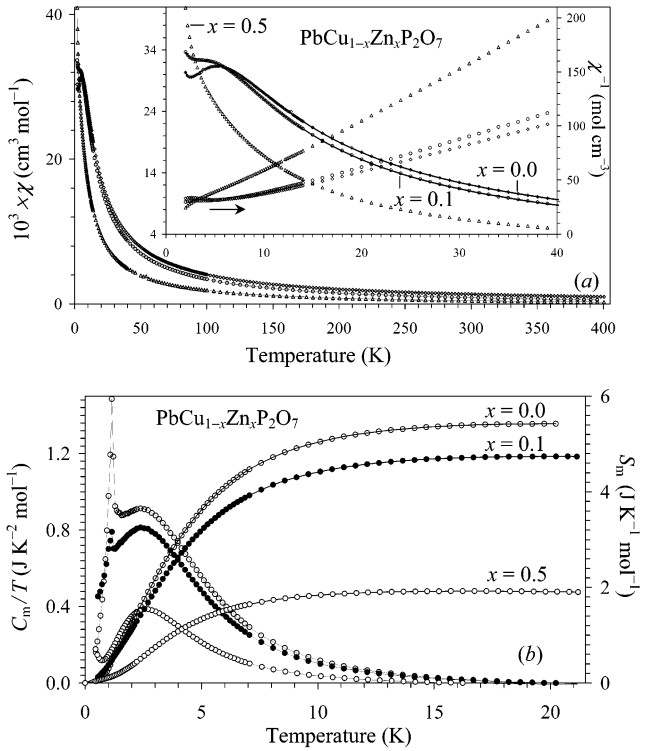

Figure 7. (a) $\chi - T$ (ZFC data) curves for $PbCu_{1-x}Zn_xP_2O_7$ with $x = 0.0$, 0.1, and 0.5. Thin solid lines between experimental points are drawn for the eye. Inset presents the enlarged fragment with the $\chi - T$ and $\chi^{-1} - T$ curves. In the insert of part a, the solid lines are the fits to eqs 2 and 3. (b) $C_m/T - T$ and $S_m - T$ curves for $PbCu_{1-x}Zn_xP_2O_7$ with $x = 0.0$, 0.1, and 0.5. Thin solid lines between experimental points are drawn for the eye.

$C_m(T)/T$ data. $C_{max} = 2.567$ J K^{-1} mol^{-1} and $T^C_{max} = 3.98$ K for $PbCu_{0.9}Zn_{0.1}P_2O_7$ and $C_{max} = 1.198$ J K^{-1} mol^{-1} and $T^C_{max} = 3.67$ K for $PbCu_{0.5}Zn_{0.5}P_2O_7$.

$S_m(T)$ decreased with increasing x. This could be attributed to the decrease in the number of spins. However, the magnitude of $S_m(T)$ for $x = 0.5$ was considerably smaller than the expected value (0.5 of the $S_m(T)$ of the $x = 0$ sample) probably because a larger percentage of S_m was gained at T_N for $PbCu_{0.5}Zn_{0.5}P_2O_7$. The $\chi(T)$ curve for $PbCu_{0.5}Zn_{0.5}P_2O_7$ did not show any maximum. This sample is not a 1D system anymore. The Curie constant (cm^{3}K/mol Cu) obtained by the fitting of the $\chi^{-1}(T)$ data for $PbCu_{1-x}Zn_xP_2O_7$ with $x = 0.1$ and 0.5 by eq 1 (given in Table 1) was almost independent of x.

In the whole temperature range, the $\chi(T)$ data for $PbCu_{0.9}Zn_{0.1}P_2O_7$ were fitted well by eqs 2 and 3 with parameters given in Table 1. The g and J/k_B values for $PbCuP_2O_7$ and $PbCu_{0.9}Zn_{0.1}P_2O_7$ were close to each other. These facts indicated that magnetic properties of $PbCu_{0.9}Zn_{0.1}P_2O_7$ were still described by the 1D chain model. Nonmagnetic impurity introduced in a 1D chain makes segments with odd and even numbers of spins. An even number segment is covered with singlets while an unpaired spin remains in an odd number segment. Therefore as expected naively, in average, two Zn^{2+} ions should give rise to one spin-$^1/_2$ in a 1D chain. It means that C_{imp} for $PbCu_{0.9}Zn_{0.1}P_2O_7$ ($x = 0.1$) should be 20 times smaller than C (0.4229 cm^{3}K/mol Cu) for $PbCuP_2O_7$. The experimentally obtained ratio of 21.7 was very close to the naively expected value.

The experimental data ($\chi(T)$ and $C_m(T)$) evidenced that magnetic properties of $SrCuP_2O_7$ and $PbCu_{1-x}Zn_xP_2O_7$ ($x = 0.0$ and 0.1) can be described well by the uniform 1D AF Heisenberg chain model. Three possible variations of $J_1 - J_4$ may result in this description: (1) J_3 is the dominant exchange constant, J_1 and J_2 are negligible, and J_4 is responsible for interchain interactions; (2) J_1 and J_2 ($J_2 \approx J_1$) are dominant, J_3 is negligible, and J_4 is responsible for interchain interactions; and (3) J_4 is the main exchange constant and $J_1 - J_3$ provide interchain interactions. It is impossible to choose the correct interaction model from the present experimental data. Inelastic neutron scattering studies on single crystals are required to determine the direction of 1D chains. However, we may choose the most probable interaction model by analyzing the geometrical parameters of Cu−O···O−Cu pathways.[26−28]

In Table 2, we summarize the geometrical parameters of M−O···O−M pathways (M is a magnetic ion) for $Sr_2Cu(PO_4)_2$, $Ba_2Cu(PO_4)_2$, $BaCuP_2O_7$, $CaCuGe_2O_6$, and $(VO)_2P_2O_7$ where the O···O contact unit is an edge of XO_4^{n-} tertahedra. The exchange constants between M atoms in these compounds are relatively strong (about 70−140 K). All the compounds in Table 2 have the following common features: (1) the M−O bonds belong to basal planes of MO_n

(26) Whangbo, M.-H.; Koo, H.-J.; Dai, D. *J. Solid State Chem.*, in press.
(27) Whangbo, M.-H.; Koo, H.-J.; Dai, D.; Jung, D. *Inorg. Chem.* **2003**, *42*, 3898−3906.
(28) Koo, H.-J.; Whangbo, M.-H.; VerNooy, P. D.; Torardi, C. C.; Marshall, W. J. *Inorg. Chem.* **2002**, *41*, 4664−4672.

Table 2. Geometrical Parameters of M−O···O−M Pathways Mediated by XO_4^{n-} Groups in Some Compounds with Strong Exchange Constants J/k_B

compd	path	bond	(Å)	angle	(deg)	J/k_B (K)
$Sr_2Cu(PO_4)_2$[29]	1 and 2	Cu−O3	1.925	Cu−O3−O3	132.0	143.6[30,31]
		O3−O3	2.500			
		Cu−O3	1.925	O3−O3−Cu	132.0	
$Ba_2Cu(PO_4)_2$[32]	1 and 2	Cu−O3	1.941	Cu−O3−O3	132.6	132.2[30,31]
		O3−O3	2.507			
		Cu−O3	1.941	O3−O3−Cu	132.6	
$BaCuP_2O_7$[33]	1	Cu−O1	1.962	Cu−O1−O3	134.7	103.6[31]
		O1−O3	2.525			
		Cu−O3	1.984	O1−O3−Cu	132.0	
	2	Cu−O5	1.939	Cu−O5−O7	127.2	
		O5−O7	2.528			
		Cu−O7	2.019	O5−O7−Cu	137.5	
$CaCuGe_2O_6$[34]	1 and 2	Cu−O1	1.943	Cu−O1−O2	131.9	67[35]
		O1−O2	2.992			
		Cu−O2	1.970	O1−O2−Cu	126.5	
$(VO)_2P_2O_7$[28]	1	V3−O17	1.941	V3−O17−O15	133.1	136[28]
		O17−O15	2.510			
		V4−O17	1.942	O17−O15−V4	132.7	
	2	V4−O16	1.944	V4−O16−O18	134.6	
		O16−O18	2.509			
		V3−O18	1.951	O16−O18−V3	131.0	
$(VO)_2P_2O_7$[28]	1	V1−O11	1.944	V1−O11−O13	128.5	94[28]
		O11−O13	2.506			
		V2−O13	1.960	O11−O13−V2	130.2	
	2	V2−O14	1.951	V2−O14−O12	129.9	
		O14−O12	2.572			
		V1−O12	1.930	O14−O12−V1	124.5	

polyhedra, (2) the M_2O_4 hexagonal ring formed by two M atoms and two O···O contact units is planar or close to planar and the O_4 ring is rectangular or almost rectangular, and (3) the optimal M−O···O bond angle is close to 132° that may just indicate that the M_2O_4 ring forms more or less regular planar hexagon. These three rules deduced from the analysis of $Sr_2Cu(PO_4)_2$, $Ba_2Cu(PO_4)_2$, $BaCuP_2O_7$, $CaCuGe_2O_6$, and $(VO)_2P_2O_7$ are in agreement with those proposed by Koo et al.[28] for $(VO)_2P_2O_7$ and related compounds; i.e., the magnitude of the super-superexchange (SSE) interaction involving paths M−O···O−M should increase as the O···O distances are decreased, as the O_4 ring formed from two O···O contact units becomes more planar, and as the basal planes of the two spin monomers become more parallel. The deviation of M−O···O bond angles from the optimal value of 132° to smaller values should strongly reduce exchange constants.

The geometrical parameters of Cu−O···O−Cu pathways responsible for J_1−J_4 in $SrCuP_2O_7$[18] and $PbCuP_2O_7$[19] are presented in Table 3. The apical Cu−O2 bonds are included in J_1 and J_3 while the Cu spins occupy $d_{x^2-y^2}$ orbitals laying on the basal planes. One of the Cu−O···O bond angles for J_1 and J_3 differs greatly from the optimal value and is even smaller than 90°. The Cu_2O_4 ring is far from planar for J_1. Therefore, all three rules formulated above were not fulfilled for J_1 and J_3, and these exchange constants should be negligible. J_2 cannot be dominant because in this case we would obtain a model of interacting dimers. However, this model was not supported by the experimental data. In addition, the Cu_2O_4 ring is far from planar for J_2, and one of the Cu−O···O bond angles for J_2 is closer to 90° (∼101°) than that for J_4 (∼114°). As a result, we conclude that J_4 should be the main exchange constant in $SrCuP_2O_7$ and $PbCuP_2O_7$. However, J_4 should be much smaller than the J values for the compounds in Table 2 because there is one Cu−O···O−Cu pathway and one of the Cu−O···O bond angles (113−114°) is considerably smaller than the optimal value. Indeed, J_4 for $SrCuP_2O_7$ and $PbCuP_2O_7$ ($J_4/k_B = 9.38$ K for $SrCuP_2O_7$ and $J_4/k_B = 8.41$ K for $PbCuP_2O_7$) was ∼10−20 times smaller than the J values in Table 2. Note that all four atoms in the Cu−O···O−Cu pathway for J_4 lay on almost one plane.

From the above discussion, we concluded that $SrCuP_2O_7$ and $PbCuP_2O_7$ should be regarded as a $S = {}^1/_2$ zigzag chain system with NN (J_4) and NNN interactions (J_5). It is hard to estimate a small effect of the NNN interaction from the susceptibility data,[14] but it is known that NNN interactions in 1D chains affect both T^C_{max} and C_{max}. From the comparison with the numerical calculation,[12] we could estimate that the J_5 value is smaller than $0.1J_4$. The small NNN interaction in this zigzag chain can be explained by the fact that the NNN interaction is mediated by two PO_4 groups sharing a corner (Figure 2), i.e., by the path Cu−O···O···O−Cu.

Thus, J_1−J_3 should be responsible for the interchain interactions. The value of interchain interaction $J_\perp/k_B$ in 1D chains can be estimated using the equation[36]

$$J_\perp/k_B = \frac{T_N}{1.28\sqrt{\ln(5.8J/(k_B T_N))}} \qquad (4)$$

This formula gives $J_\perp/k_B = 0.68$ K for $SrCuP_2O_7$ and $J_\perp/k_B = 0.46$ K for $PbCuP_2O_7$. Interchain interactions are ∼10−20 times smaller than J_4.

In conclusion, we characterized $SrCuP_2O_7$ and $PbCuP_2O_7$ by magnetic susceptibility, specific heat, and thermal analy-

Table 3. Geometrical Parameters of Cu−O···O−Cu Pathways Responsible for J_1−J_4 in $SrCuP_2O_7$[18] and $PbCuP_2O_7$[19]

		bond (Å)			angle (deg)		
J	path		$SrCuP_2O_7$	$PbCuP_2O_7$		$SrCuP_2O_7$	$PbCuP_2O_7$
J_1	1 and 2	Cu−O2	2.284	2.275	Cu−O2−O3	88.7	89.7
		O2−O3	2.537	2.534			
		Cu−O3	1.963	1.975	O2−O3−Cu	110.1	110.3
J_2	1 and 2	Cu−O1	1.978	1.951	Cu−O1−O3	140.5	142.1
		O1−O3	2.513	2.536			
		Cu−O3	1.963	1.975	O1−O3−Cu	100.6	100.9
J_3	1	Cu−O1	1.978	1.951	Cu−O1−O2	85.8	88.2
		O1−O2	2.562	2.544			
		Cu−O2	2.284	2.275	O1−O2−Cu	147.8	149.6
J_4	1	Cu−O5	1.910	2.005	Cu−O5−O6	168.2	167.6
		O5−O6	2.453	2.396			
		Cu−O6	2.050	2.042	O5−O6−Cu	112.8	114.0

sis. We observed short-range and long-range magnetic ordering in these compounds and explained the experimental data by the presence of the uniform 1D $S = {}^1/_2$ AF zigzag chains with almost negligible NNN interactions.

(29) Belik, A. A.; Malakho, A. P.; Lazoryak, B. I.; Khasanov, S. S. *J. Solid State Chem.* **2002**, *163*, 121−131.
(30) Belik, A. A.; Azuma, M.; Takano, M. *J. Solid State Chem.*, in press.
(31) Belik, A. A.; Azuma, M.; Takano, M. *J. Magn. Magn. Mater.*, in press.
(32) Etheredge, K. M. S.; Hwu, S.-J. *Inorg. Chem.* **1996**, *35*, 1474−1477.
(33) Moqine, A.; Boukhari, A.; Holt, E. M. *Acta Crystallogr., Sect. C* **1991**, *47*, 2294−2297.
(34) Behruzi, M.; Breuer, K. H.; Eysel, W. *Z. Kristallogr.* **1986**, *176*, 205−217.
(35) Valentí, R.; Saha-Dasgupta, T.; Gros, C. *Phys. Rev. B* **2002**, *66*, 054426-1−054426-4.
(36) Schulz, H. J. *Phys. Rev. Lett.* **1996**, *77*, 2790−2793.

Acknowledgment. The authors express their thanks to the Ministry of Education, Culture, Sports, Science and Technology, Japan, for Grants-in-Aid No. 12CE2005, for COE Research on Elements Science, No. 14204070, and for 21COE on Kyoto Alliance for Chemistry.

Supporting Information Available: Experimental, calculated, and difference XRD patterns and lattice parameters for $SrCuP_2O_7$, $SrZnP_2O_7$, and $PbCu_{1-x}Zn_xP_2O_7$ ($x = 0$, 0.1, 0.5, and 1.0) (Figures S1-S6). $C_m(T)$ curves for $PbCu_{1-x}Zn_xP_2O_7$ ($x = 0$, 0.1, and 0.5) (Figure S7). DTA curves for $SrCuP_2O_7$ and $PbCuP_2O_7$ (Figure S8). This material is available free of charge via the Internet at http://pubs.acs.org.

IC034825W